

## Article

# Comparative Numerical Study of PM<sub>2.5</sub> in Exit-and-Entrance Areas Associated with Transboundary Transport over China, Japan, and Korea

Cheol-Hee Kim <sup>1,\*</sup>, Fan Meng <sup>2,\*</sup>, Mizuo Kajino <sup>3</sup>, Jaehyun Lim <sup>4,\*</sup>, Wei Tang <sup>2</sup>, Jong-Jae Lee <sup>5</sup>, Yusuke Kiriyama <sup>6</sup>, Jung-Hun Woo <sup>7</sup>, Keiichi Sato <sup>6</sup>, Toshihiro Kitada <sup>8</sup>, Hiroaki Minoura <sup>6</sup>, Jiyoung Kim <sup>4</sup>, Kyoung-Bin Lee <sup>9</sup>, Soona Roh <sup>4</sup>, Hyun-Young Jo <sup>10</sup> and Yu-Jin Jo <sup>1</sup>

- <sup>1</sup> Department of Atmospheric Sciences, Pusan National University, Busan 46241, Korea; yujinjo@pusan.ac.kr  
<sup>2</sup> Institute of Atmospheric Environment, Chinese Research Academy of Environmental Sciences (CRAES), Beijing 100012, China; tangwei@craes.org.cn  
<sup>3</sup> Meteorological Research Institute (MRI), Japan Meteorological Agency (JMA), Tsukuba 305-0052, Japan; kajino@mri-jma.go.jp  
<sup>4</sup> Climate & Air Quality Research Department, National Institute of Environmental Research (NIER), Incheon 404170, Korea; jykim77@korea.kr (J.K.); glaycat@hanmail.net (S.R.)  
<sup>5</sup> Ulsan National Institute of Science and Technology, School of Urban and Environmental Engineering, Ulsan 44919, Korea; leejongjae@pusan.ac.kr  
<sup>6</sup> Asia Center for Air Pollution Research (ACAP), Niigata 950-2144, Japan; kiriyama@acap.asia (Y.K.); ksato@acap.asia (K.S.); dsc\_mino@yahoo.co.jp (H.M.)  
<sup>7</sup> Department of Civil and Environmental Engineering, Konkuk University, Seoul 05029, Korea; jwoo@konkuk.ac.kr  
<sup>8</sup> Department of Applied Chemistry and Life Science, Toyohashi University of Technology, Toyohashi 441-8580, Japan; tk032@edu.tut.ac.jp  
<sup>9</sup> Emission Inventory Management Team, National Air Emission Inventory and Research Center, Osong 28166, Korea; llkb0510@korea.kr  
<sup>10</sup> Institute of Environmental Studies, Pusan National University, Busan 46241, Korea; hycho@pusan.ac.kr  
\* Correspondence: chkim2@pusan.ac.kr (C.-H.K.); mengfan@craes.org.cn (F.M.); dr4earth@korea.kr (J.L.)



**Citation:** Kim, C.-H.; Meng, F.; Kajino, M.; Lim, J.; Tang, W.; Lee, J.-J.; Kiriyama, Y.; Woo, J.-H.; Sato, K.; Kitada, T.; et al. Comparative Numerical Study of PM<sub>2.5</sub> in Exit-and-Entrance Areas Associated with Transboundary Transport over China, Japan, and Korea. *Atmosphere* **2021**, *12*, 469. <https://doi.org/10.3390/atmos12040469>

Academic Editor: Chuen-Jinn Tsai

Received: 7 March 2021

Accepted: 2 April 2021

Published: 8 April 2021

**Publisher's Note:** MDPI stays neutral with regard to jurisdictional claims in published maps and institutional affiliations.



**Copyright:** © 2021 by the authors. Licensee MDPI, Basel, Switzerland. This article is an open access article distributed under the terms and conditions of the Creative Commons Attribution (CC BY) license (<https://creativecommons.org/licenses/by/4.0/>).

**Abstract:** We report the results of year-long PM<sub>2.5</sub> (particulate matter less than 2.5  $\mu\text{m}$  in diameter) simulations over Northeast Asia for the base year of 2013 under the framework of the Long-range Transboundary Air Pollutants in Northeast Asia (LTP) project. LTP is a tripartite project launched by China, Japan, and Korea for cooperative monitoring and modeling of the long-range transport (LRT) of air pollutants. In the modeling aspect in the LTP project, each country's modeling group employs its own original air quality model and options. The three regional air quality models employed by the modeling groups are WRF-CAMx, NHM-RAQM2, and WRF-CMAQ. PM<sub>2.5</sub> concentrations were simulated in remote exit-and-entrance areas associated with the LRT process over China, Japan, and Korea. The results showed apparent bias that remains unexplored due to a series of uncertainties from emission estimates and inherent model limitations. The simulated PM<sub>10</sub> levels at seven remote exit-and-entrance sites were underestimated with the normalized mean bias of  $0.4 \pm 0.2$ . Among the four chemical components of PM<sub>2.5</sub> (SO<sub>4</sub><sup>2-</sup>, NO<sub>3</sub><sup>-</sup>, organic carbon (OC), and elemental carbon (EC)), the largest inter-model variability was in OC, with the second largest discrepancy in NO<sub>3</sub><sup>-</sup>. Our simulation results also indicated that under considerable SO<sub>4</sub><sup>2-</sup> levels, favorable environments for ammonium nitrate formation were found in exit-and-entrance areas between China and Korea, and gas-aerosol partitioning for semi-volatile species of ammonium nitrate could be fully achieved prior to arrival at the entrance areas. Other chemical characteristics, including NO<sub>3</sub><sup>-</sup>/SO<sub>4</sub><sup>2-</sup> and OC/EC ratios, are discussed to diagnose the LRT characteristics of PM<sub>2.5</sub> in exit-and-entrance areas associated with transboundary transport over China, Japan, and Korea.

**Keywords:** model intercomparison; transboundary air pollutants in Northeast Asia (LTP); PM<sub>2.5</sub> simulation; Northeast Asia

## 1. Introduction

PM<sub>2.5</sub> (ultrafine particulate matter (PM) with a diameter of less than 2.5  $\mu\text{m}$ ) has adverse effects on both climate radiative forcing and the human body, leading to numerous respiratory diseases. The International Research Agency on Cancer, a specialized institution of the World Health Organization, designates PM<sub>2.5</sub> as a carcinogen of the highest level. In addition, PM<sub>2.5</sub> is closely associated with long-range transport (LRT) processes [1,2] and is therefore of long-term international concern. Over Northeast Asia, PM<sub>2.5</sub> pollution is an issue of the highest priority, as local emissions can markedly affect the environments of downwind areas through LRT in combination with complex transport, transformation, deposition, and removal processes. Although many site-specific studies of PM and its gas-phase precursors are underway [3–5], model-based analysis of the most efficient emission mitigation methodology for PM<sub>2.5</sub> and its applicability in light of the LRT process is still lacking.

PM<sub>2.5</sub> formation processes, especially secondary formation, during LRT are highly complicated. Gaseous precursors such as SO<sub>2</sub>, NO<sub>2</sub>, and volatile organic compounds (VOCs) may be converted through photo-oxidation during LRT, and in turn, semi-volatile condensable vapors can be formed via the secondary aerosol formation process during (as well as before or after) the LRT process [6,7]. Such secondary aerosol formation can occur in two manners: homogeneous and heterogeneous formation. Homogeneous and heterogeneous reactions occur via many pathways, depending on how the materials comprising PM<sub>2.5</sub> were generated and the extent to which the precursors were exposed to NH<sub>3</sub> in the environment. Over Northeast Asia, although PM<sub>2.5</sub> over major metropolitan areas has been frequently studied, remote and near-border areas (referred to as “exit-and-entrance” areas in this study) over Northeast Asia are lacking in data, as the monitoring of both inflow and outflow areas requires international cooperation.

To establish international cooperation and clarify the source–receptor relationships (SRRs) among nations, combined research groups are organized and activated through research programs. One example of such a program is “Long-range Transboundary Air Pollutants in Northeast Asia (LTP),” which was established by the governments of three countries: China, Japan, and Korea. LTP was launched in 1995 and collaborative research has been performed by the three countries for monitoring and modeling transboundary air pollutants over Northeast Asia, focusing specifically on exit-and-entrance areas [8–11]. In this collaborative project, modeling and monitoring studies have been conducted to support long-term SRR calculation.

In the recent LTP framework, model intercomparison studies on the simulation of PM<sub>2.5</sub> concentrations have a standard base year of 2013, the starting year of Chinese 5-year massive emission reduction implementation over the major cities, and the diagnosis of PM<sub>2.5</sub> over remote areas is provided, focusing on exit-and-entrance areas associated with LRT processes out of, into, and among the three countries. In the LTP modeling framework, three modeling groups from China, Japan, and Korea each use their own conventional air quality models with the appropriate options (e.g., physical and chemical treatments, initial and boundary conditions, parameterization processes, and other transport and removal processes). At an annual meeting, inter-model variabilities including those related to emission inventories, meteorological and chemical fields, removal processes, and PM conversion rates were addressed.

In this paper, we present the outputs of modeling intercomparison results produced by researchers of the LTP modeling project. An overview of the major findings obtained through modeling and a comparison among the three models for the base year of 2013 is presented. The emphasis is on monitoring of remote exit-and-entrance areas through which transboundary air pollutants pass over China, Japan, and Korea. We also explored PM<sub>2.5</sub> composition through simulated gas-to-aerosol partitioning of inorganic NO<sub>3</sub><sup>−</sup>, NO<sub>3</sub><sup>−</sup>/SO<sub>4</sub><sup>2+</sup>, and organic carbon to elemental carbon (OC/EC) ratios in exit-and-entrance areas during LRT. We expect that our results for the base year of 2013 serve as a useful reference for interpreting PM<sub>2.5</sub> base levels prior to the implementation of Chinese emission

mitigation strategies, because in 2013, the Chinese government began to implement the first 5-year Clean Air Action Plan [12] for mitigating PM pollution.

## 2. Models and Monitoring Sites

### 2.1. Modeling Framework of the LTP Project

The shared domain of the three models used here covers 20–50° N and 100–150° E, including the entirety of Korea and Japan, most of China, and parts of Mongolia, Russia, and some Southeast Asian countries (Figure 1). The three air quality models are all three-dimensional Eulerian models that include transport, chemistry, and removal modules, as well as individual three-dimensional meteorological numerical models. The meteorological fields are provided in an individual manner with their own meteorological drivers. As the members of the LTP project agreed to accept the original models without specifying any options, such as resolution or physical and chemical parameters, individual modeling groups do not necessarily use the same model parameters or input data. Anthropogenic emissions are recommended as the unified input data; however, lax specifications regarding emission inventories were agreed upon to accommodate various contributors to this project.

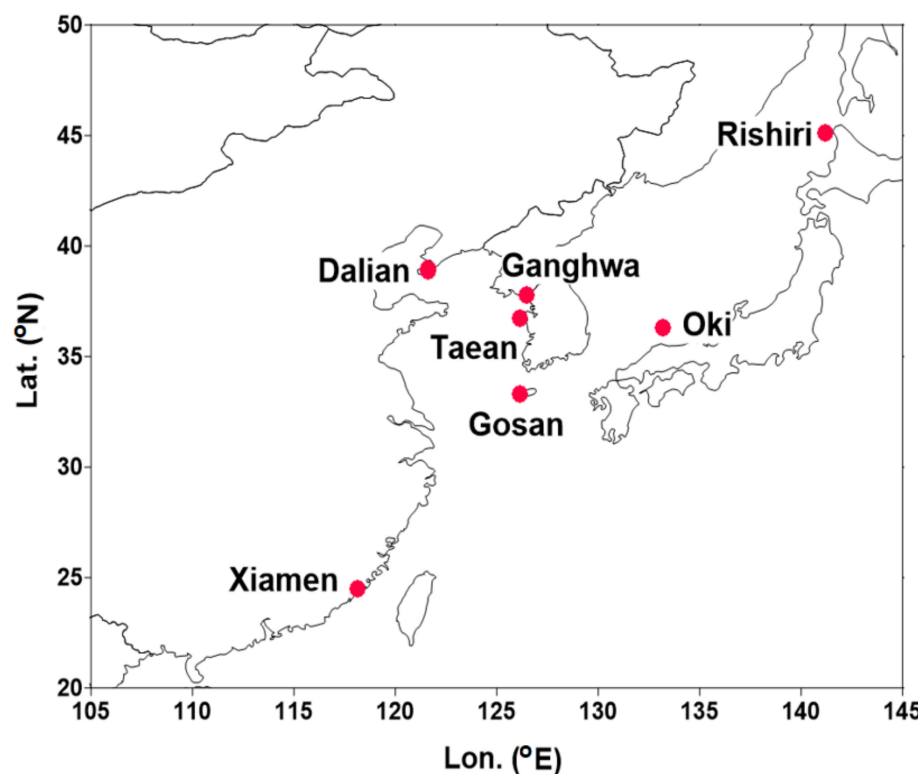


**Figure 1.** Locations of seven monitoring sites representing exit-and-entrance areas of transboundary transport over China, Japan, and Korea. The longitudes and latitudes of the seven sites are presented in Supplementary Table S1.

The three models used in LTP are the Weather Research and Forecasting (WRF)-Comprehensive Air Quality Model with Extensions (CAMx), Non-Hydrostatic Model (NHM)-Regional Air Quality Model2 (RAQM2), and WRF-Community Multiscale Air Quality Modeling System (CMAQ) (hereafter referred to as WRF-CAMx, NHM-RAQM2, and WRF-CMAQ, respectively), employed by China, Japan, and Korea, respectively. Each modeling system is abbreviated in the form of “A-B”, with the meteorological model (A) and chemical transport model (B), combined with a hyphen (-), for convenience in the present study. The meteorological and chemical models, WRF, CAMx, NHM, RAQM2, and CMAQ, have all been used across numerous research communities [13–20]. The individual

models employed zero initial conditions and default profiles of boundary conditions. Detailed information on each of these three models is provided in Table 1.

**Table 1.** Descriptions of the physical and chemical parameters of three models: WRF-CMAx (Weather Research and Forecasting-Comprehensive Air Quality Model with Extensions), NHM-RAQM2 (Non-Hydrostatic Model-Regional Air Quality Model2), and WRF-CMAQ (Weather Research and Forecasting-Community Multi-scale Air Quality Modeling System), employed by the Chinese, Japanese, and Korean modeling research groups, respectively.

	China	Japan	Korea
Air quality model	CAMx	RAQM2	CMAQ
Model domain		20–50° N, 100–150° E	
Map projection		Lambert conformal projection	
Model run		Off-line run	
Vertical coordinate	σ coordinate	Terrain following	Terrain following
Horizontal resolution		36 km (220 × 140 grids)	
Vertical layers	14	20	23
Gas phase chemistry	SAPRC 99 mechanism (common to three models)		
Chemical species		93 reactions, 36 species with 11 photochemistry	
Aqueous chemistry		RADM Chemistry	
Dry deposition	Wesely's method	Modified by Zhang et al. (2003) [13]	RADM module
Wet deposition	RADM module	Kajino et al. (2012) [18]	RADM module
Aerosol thermodynamics	ISORROPIA	ISORROPIA2	AERO5
Emission	REAS + MEIC	CREATE-2013	CREATE-2013
Vertical Diffusivity	Brost's method	1.5 order TKE	ACM2
Meteorological Model	WRF	NHM	WRF
Basic equation		Compressible/non-hydrostatic equation	
Horizontal resolution		36 km (220 × 140 grids)	
Horizontal grid	Arakawa-B	Arakawa-C	Arakawa-C
Domain structure		Non-nested grid structure for all three models	
Vertical coordinate	Terrain following pressure	Terrain following height	Terrain following height
Vertical layers	34	50	43
Data assimilation	FDDA	JCDAS	FDDA
Cumulus parameterization	Kain-Fritsch scheme	Arakawa-Shubert scheme	Kain-Fritsch scheme
TKE closure	1.5-order TKE	MYNN2	1.5-order TKE
PBL scheme	YSU PBL scheme	MYNN2	YSU PBL scheme
Microphysics	WSM3	Mixed-phase 2-moment	WSM3
Radiation	RRTM Longwave radiation scheme (common to three models)		
Soil layer	5-layer soil model	5-layer soil model	Multi-layer soil model
Land use type	USGS EROS (13 categories)	EROS (12 categories)	USGS EROS (13 categories)

## 2.2. Observation Sites in the Exit-and-Entrance Areas

In-situ surface measurements were collected at seven exit-and-entrance sites: Fujiazhan in Dalian (China), Xiamen (China), Ganghwa, Taean, and Gosan (Korea), and Oki and Rishiri (Japan). These sites are located in remote areas in near-border areas of China, Japan, and Korea, and have been recognized as exit-and-entrance sites to mon-

itor both inflow and outflow of air pollutants over Northeast Asia. The locations and characteristics of these seven sites are illustrated in Figure 1 and listed in Supplementary Table S1. It should also be noted that these seven sites are recognized as monitoring sites over exit or entrance areas decided by three governments in the LTP framework, which are associated with transboundary transport over three countries: China, Japan, and Korea. Therefore, measurements from sites other than these seven sites are beyond the content of the current study.

### 2.3. Emission Data Used

The anthropogenic emission inventory employed by NHM-RAQM2 and WRF-CMAQ is the Comprehensive Regional Emissions for Atmospheric Transport Experiments (CREATE), which was developed by the National Institute of Environmental Research and Kunkuk University of Korea in 2013. The CREATE data for the base year of 2013 (CREATE-2013) are based on GAINS/BlueSky emissions model. The 0.5-degree gridded monthly global emissions data of GAINS-Asia were mosaicked for 2013 using the CAPSS (Clean Air Policy Support System) emission inventory and generated hourly emissions with a horizontal resolution of 36 km over the entire LTP domain (Figure 1). The anthropogenic emissions dataset CREATE was used in the 2015 Megacity Air Pollution Studies—Seoul Project [7,21], and the Korea and USA Air Quality Campaign Project, launched in 2016. It contains data on anthropogenic  $\text{NO}_x$ ,  $\text{SO}_2$ ,  $\text{NH}_3$ , non-methane VOC (NMVOC), black carbon (BC), and primary organic aerosol (POA) emissions. The detailed CREATE-2013 emission strengths for  $\text{SO}_2$ ,  $\text{NO}_x$ , VOCs,  $\text{NH}_3$ , and primary  $\text{PM}_{2.5}$  for China, Japan, and Korea are listed separately in Supplementary Table S2, and the gridded emission spatial distributions (ton/year/grid) of CREATE-2013 are shown in Supplementary Figure S1.

WRF-CAMx employs a Chinese emissions inventory originally inferred from the Multi-resolution Emission Inventory (MEIC) for China and the Regional Emission Inventory in Asia (REAS ver. 2) [22] for areas outside of China. Biogenic emissions are considered in WRF-CAMx and NHM-RAQM2, which are generated by MEGAN2. In addition, NHM-RAQM2 employs both volcanic emissions over Japan and the Global Fire Emissions Database (GFED3) [23] for open biomass burning emissions of  $\text{NO}_x$ ,  $\text{SO}_2$ , NMVOCs, BC, and POA.

## 3. Results

### 3.1. Meteorological Fields and $\text{SO}_2$ and $\text{NO}_x$ Gas Species

The spatial distributions of the monthly mean temperature and wind fields simulated by the three models for representative months of four seasons—i.e., January, April, July, and October—are shown in Supplementary Figures S2 and S3, respectively. Monthly mean temperatures exhibited a similar distribution in all models, with strong shared variations. The wind fields also exhibited close resemblance in all three models, showing that northwest air currents prevailed over northeast China, Korea, and Japan in spring (April) and winter (January), whereas southerlies prevailed over southern China, Korea, and Japan in summer (July) due to the East Asia summer monsoon over the Pacific Ocean, and the pattern in autumn (October) was similar to that in the winter, but with much lower wind speeds.

Notably, all three models used in this study overestimated the surface wind speed relative to surface observations in Seoul by factors of 1.5–2.2 (Supplementary Figure S4), whereas non-surface (i.e., 850 haPa) wind speed exhibited fairly good agreement (data not shown). This pattern is frequently observed in major cities in Northeast Asia, indicating that overprediction of near-ground-level wind speed is one of the important factors affecting  $\text{PM}_{2.5}$  prediction performance over Northeast Asia. Other meteorological variables, such as relative humidity and pressure, were well-aligned with observation data at measurement sites including Beijing, Tianjin, and Hubei. Some models slightly underestimated relative humidity, and all three models' pressure simulations provided small overestimates in those

three cities relative to actual observations. However, overall, the simulated meteorological fields were credible, with no significant biases and low root mean square errors.

The distributions of gaseous  $\text{SO}_2$  and  $\text{NO}_2$  are shown in Supplementary Figures S5 and S6 respectively, for the representative months of January, April, July, and October. The spatial distributions of gaseous  $\text{SO}_2$  were almost identical to those of  $\text{SO}_2$  emissions, as illustrated in Supplementary Figure S1. All models indicated the same general pattern of gaseous  $\text{SO}_2$ : higher in winter and lower in summer (Supplementary Figure S5), mainly due to the emission characteristics, as discussed in the previous studies [9,10]. Relatively, WRF-CAMx predicted lower levels of  $\text{SO}_2$  than the others in January, particularly in Beijing and surrounding urban areas (Supplementary Figure S5). High  $\text{SO}_2$  concentrations also occurred in three areas of Mainland China (i.e., northern China)—namely, the Shangxi, Shangdong, and Beijing-Tianjin metropolitan areas and their surrounding provinces, which all correspond to high- $\text{SO}_2$  emission areas. In China, the center of high  $\text{SO}_2$  concentrations appeared to be in northeast China, namely the Chongqing area, the Yangzi River Delta, and Hubei Province, with levels reaching above 50 ppb. In Korea, Pusan had the highest  $\text{SO}_2$  concentration, at approximately 15 ppb, and most areas of Japan had significantly lower  $\text{SO}_2$  concentrations. WRF-CAMx simulated lower peaks than the other two models by less than 10 ppb, especially in and around large emission sources (Supplementary Figure S1). The general trends show similar statistical results to previous LTP studies for the base year of 2002 [9,10].

The  $\text{NO}_2$  distributions, shown in Supplementary Figure S6, also indicate distribution patterns similar to emission patterns (Supplementary Figure S1). In Korea and Japan, the highest  $\text{NO}_2$  concentrations were at the same levels as those in Mainland China. However, inter-model variability for  $\text{NO}_2$  was higher than that for  $\text{SO}_2$ . NHM-RAQM2 predicted lower monthly mean  $\text{SO}_2$  and  $\text{NO}_2$  values and greater conversion from the gas to aerosol phase for both species. The three models all predicted elevated  $\text{NO}_2$  concentrations in Chongqing, the Northeast China Plain, Seoul in Korea, and Osaka in Japan, which all approached ~30 ppb. The spatial distributions of  $\text{NO}_2$  over Mainland China resembled those of  $\text{SO}_2$ , and regions of high  $\text{NO}_2$  concentrations occurred at locations near those of  $\text{SO}_2$  in Mainland China. However, some differences were found relative to  $\text{SO}_2$  in Korea and Japan. For example, higher  $\text{NO}_2$  concentrations were simulated in the metropolitan areas of Seoul and Pusan, Korea, and in Tokyo, Japan, in 2013 due to reduced coal consumption, in contrast to China (Supplementary Figures S5 and S6).

### 3.2. Concentrations of $\text{PM}_{2.5}$ and Its Chemical Components

As various chemical species of  $\text{PM}_{2.5}$  were included in each of the three models, we defined  $\text{PM}_{2.5}$  as comprising the following species:

$$[\text{PM}_{2.5}] = [\text{Primary PM}_{2.5}] + [\text{SO}_4^{2-}] + [\text{NO}_3^-] + [\text{NH}_4^+] + [\text{EC}] + [\text{OC}] \quad (1)$$

However, NHM-RAQM2 employed a different definition of  $\text{PM}_{2.5}$ , namely the summation of submicron-size anthropogenic aerosols ( $\text{SO}_4^{2-}$ ,  $\text{NH}_4^+$ ,  $\text{NO}_3^-$ , and  $\text{Cl}^-$ ) in the Aitken mode category, unidentified components (UID), organic aerosols (OAs),  $\text{SO}_4^{2-}$ ,  $\text{NH}_4^+$ ,  $\text{NO}_3^-$ , and  $\text{Cl}^-$  in the accumulation mode category, UID, BC, OA,  $\text{SO}_4^{2-}$ ,  $\text{NH}_4^+$ ,  $\text{NO}_3^-$ , and  $\text{Cl}^-$  in the soot aggregate category, and BC, OA,  $\text{SO}_4^{2-}$ , and  $\text{NH}_4^+$  in the coarse mode category.  $\text{PM}_{10}$  in NHM-RAQM2 includes  $\text{PM}_{2.5}$ , UID, mineral dust (DU), sea salt (SS), and  $\text{Cl}^-$  in the coarse mode category. UID in the coarse mode is defined as primary  $\text{PM}_{10}$  emission and DU, with SS and  $\text{Cl}^-$  assumed to have originated from sea-salt particles. These natural components of larger sizes (relative to  $\text{PM}_{2.5}$ ) were also considered.

$\text{PM}_{2.5}$  mass concentrations: Figure 2 shows the spatial distributions of monthly average  $\text{PM}_{2.5}$  mass concentrations for each of four representative months: January, April, July, and October. The three models simulated peak  $\text{PM}_{2.5}$  concentrations over northeast, southwest, and central China that reached approximately  $\sim 100 \mu\text{g}/\text{m}^3$ , with the highest peaks in January. Lower peaks were simulated at approximately  $30 \mu\text{g}/\text{m}^3$  in Korea, and at approximately  $15 \mu\text{g}/\text{m}^3$  in Japan. Over Northeast Asia, two relatively higher areas

were observed—a larger area covering eastern China from Beijing to Shanghai, and a smaller area comprising Chongqing and its surroundings in southwestern China, and these areas tended to have the highest  $\text{SO}_2$  and  $\text{NO}_x$  concentrations in Mainland China (Supplementary Figures S5 and S6). The spatial distribution patterns in July (Figure 2) appear to reflect two complicated factors: lower emissions and scavenging effects [9,10], which outweigh the effects of secondary photochemical PM generation during summer. For these reasons, the distributions of  $\text{PM}_{10}$  also exhibited the same seasonality as those for  $\text{SO}_2$  and  $\text{NO}_x$ , with high values in winter and low values in summer. One important difference among the three models was found over southern Russia, where  $\text{PM}_{2.5}$  with broad features and extremely high levels are simulated by NHM-RAQM2. As only NHM-RAQM2 considered emissions from biomass burning, biomass usage causes distinctive  $\text{PM}_{2.5}$  variations among models in 2013, driven by primary OC emission due to biomass burning over southern Russia.

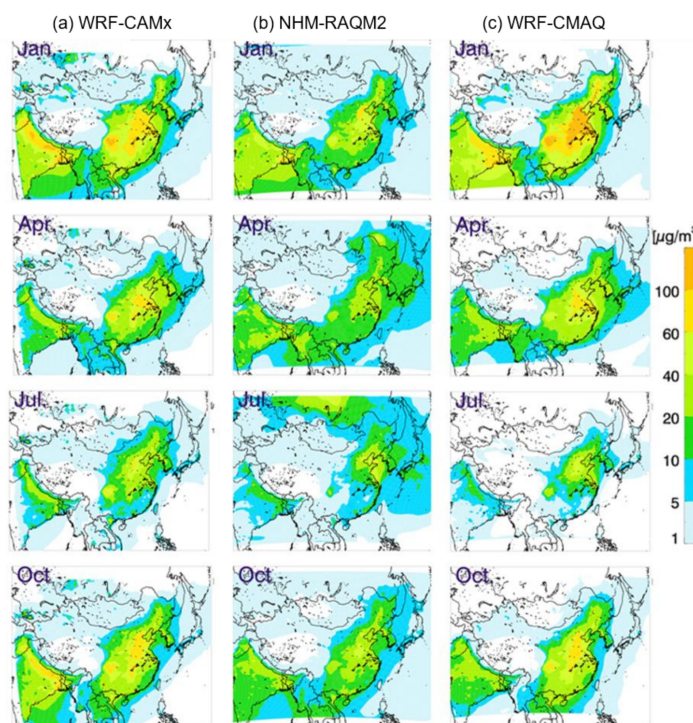


**Figure 2.** Spatial distributions of monthly average  $\text{PM}_{2.5}$  concentrations ( $\mu\text{g}/\text{m}^3$ ) for January, April, July, and October 2013. The three air quality models are (a) WRF-CAMx, (b) NHM-RAQM2, and (c) WRF-CMAQ, employed by China, Japan, and Korea, respectively.

$\text{SO}_4^{2-}$  inorganic component: The spatial distributions of  $\text{SO}_4^{2-}$  concentrations are shown in the four representative months. High  $\text{SO}_4^{2-}$  levels were simulated in northern China, with maximum of  $42.6 \mu\text{g}/\text{m}^3$  (by WRF-CAMx),  $48.1 \mu\text{g}/\text{m}^3$  (by NHM-RAQM2), and  $38.3 \mu\text{g}/\text{m}^3$  (by WRF-CMAQ) in July. Compared with the strong seasonality exhibited by gaseous  $\text{SO}_2$  concentrations (Supplementary Figure S5), those of  $\text{SO}_4^{2-}$  exhibited no particular seasonal pattern. This lower variation was ascribed to the offset between two factors in summer—scavenging effects and secondary inorganic aerosol (SIA) formation through the conversion of  $\text{SO}_2$  to  $\text{SO}_4^{2-}$  due to strong photochemical reactions.

Our calculations indicated that the simulated conversion ratio of sulfur ( $F_S = [\text{SO}_4^{2-}] / ([\text{SO}_2] + [\text{SO}_4^{2-}])$ ) ranged from  $0.37 \sim 0.39$  at seven exit-and-entrance sites, well compared with 0.3 to 0.5 calculated for the year 2002 [10] over the entire LTP domain. Among the three models tested here, NHM-RAQM2 simulated relatively high  $F_S$  values ( $0.39 \pm 0.24$ ) compared with those from WRF-CAMx ( $0.37 \pm 0.24$ ) and WRF-CMAQ ( $0.37 \pm 0.26$ ), yielding relatively high  $\text{SO}_4^{2-}$  levels in July (Figure 3).

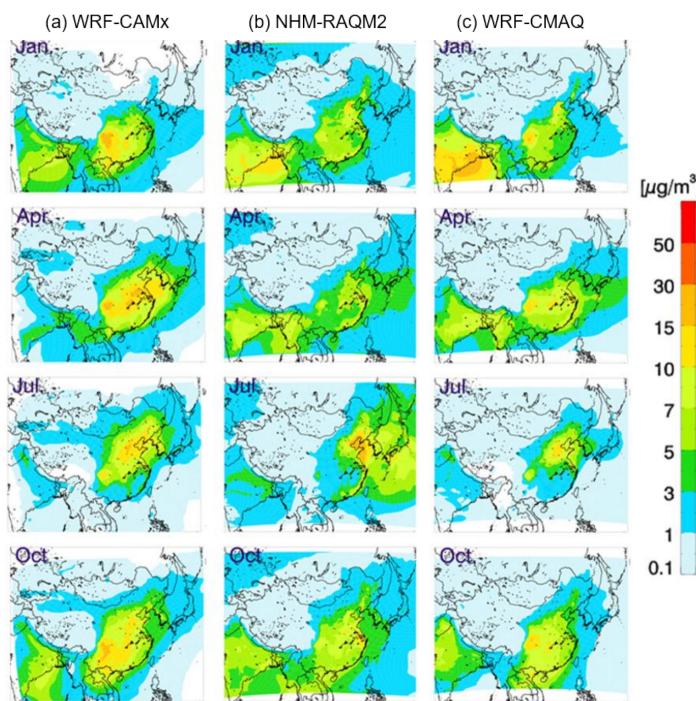


**Figure 3.** As in Figure 2, but for  $\text{SO}_4^{2-}$  concentrations ( $\mu\text{g}/\text{m}^3$ ).

$\text{NO}_3^-$  inorganic component: Figure 4 shows the spatial distributions of  $\text{NO}_3^-$  concentrations. The results for  $\text{NO}_3^-$  indicated higher inter-model biases than  $\text{SO}_4^{2-}$ , the causes of which were less clear than those of the  $\text{SO}_4^{2-}$  component, but these were likely due to uncertainties in either emission estimates or inherent SIA module limitations. Among the three models, WRF-CAMx produced the most severe underestimation, except during winter. NHM-RAQM2 simulated small seasonal variations, with consistent peaks in some areas and nearly uniform maximum  $\text{NO}_3^-$  levels greater than  $20 \mu\text{g}/\text{m}^3$  in all seasons.

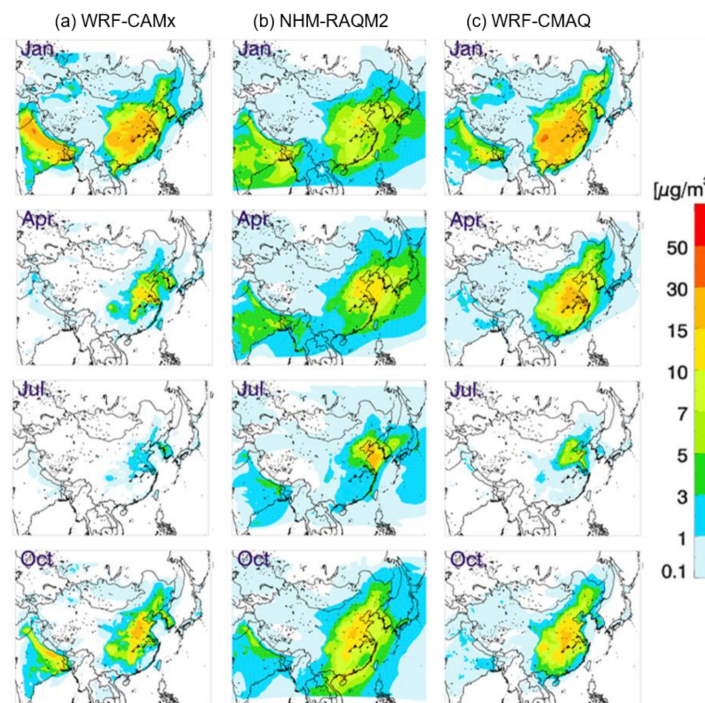


**Figure 4.** As in Figure 2, but for  $\text{NO}_3^-$  concentrations ( $\mu\text{g}/\text{m}^3$ ).

In the present study, the fractional contributions of  $\text{NO}_3^-$  to  $\text{PM}_{2.5}$  mass concentration were approximately 30%. This fraction is comparable to that of  $\text{SO}_4^{2-}$  but much greater than those of OC and EC. We did not investigate total reactive nitrogen ( $\text{NO}_y$ ), that is defined as the sum of  $\text{NO}_x$  and its oxidized products ( $\text{HNO}_3 + \text{NO}_3^-$ , peroxyacetyl nitrate, and others), but here, we conventionally calculated  $F_N$  ( $= [\text{NO}_3^-]/([\text{NO}_2] + [\text{NO}_3^-])$ ) in the same manner as for  $F_S$ . The results showed that the  $F_N$  range calculated at seven exit-and-entrance sites was  $0.27 \pm 0.21$ . However, larger inter-model variability was found at seven sites. Simulated  $F_N$  by NHM-RAQM2 ( $0.46 \pm 0.22$ ) was higher than those shown by either WRF-CAMx ( $F_N = 0.12 \pm 0.08$ ) or WRF-CMAQ ( $F_N = 0.22 \pm 0.16$ ) by a factor of more than 2. This implies that higher transboundary  $\text{NO}_3^-$  concentrations than those by WRF-CAMx and WRF-CMAQ was predicted due to the most extensive oxidization from  $\text{NO}_2$  to  $\text{NO}_3^-$  by NHM-RAQM2 (Figure 4 and Supplementary Figure S5) especially in April and July, at atmospheric levels of  $\text{NH}_4^+$  (Supplementary Figure S7). This finding also indicates that inherent potential model uncertainties in secondary ammonium nitrate formation remain limited and unexplored, resulting in the high inter-model variability and, as a result, affecting prediction performance in the  $\text{NO}_2$  to  $\text{NO}_3^-$  conversion process over Northeast Asia.

Uncertainty in simulating the gas-to-aerosol conversion process is related to the thermodynamic equilibrium module and inorganic aerosol formation mechanisms involving interactions between  $\text{SO}_4^{2-}$ ,  $\text{NO}_3^-$ , and  $\text{NH}_4^+$  species. In the present study, SIA ( $\text{SO}_4^{2-}-\text{NO}_3^--\text{NH}_4^+$ ) is the main contributor to  $\text{PM}_{2.5}$  mass concentrations; therefore, potential uncertainty caused by employing different SIA formation modules (ISOROPIA, MADMS, and AERO5, as indicated in Table 1) cannot be excluded.

**Organic Carbon (OC) component:** Figure 5 shows the spatial distributions of OC simulated by the three models. Secondary organic aerosol (SOA) formation occurs actively in summer, when environmental conditions are favorable, namely high temperature and radiation [24,25]. Our simulations revealed unexpected seasonal variations with the opposite pattern—lower in summer and higher in winter [26,27]. This pattern is driven by both meteorological factors and higher emissions of primary organic aerosols in winter. Our simulations generally predicted levels below  $10 \mu\text{g}/\text{m}^3$ , but discrepancies among the three models were large.

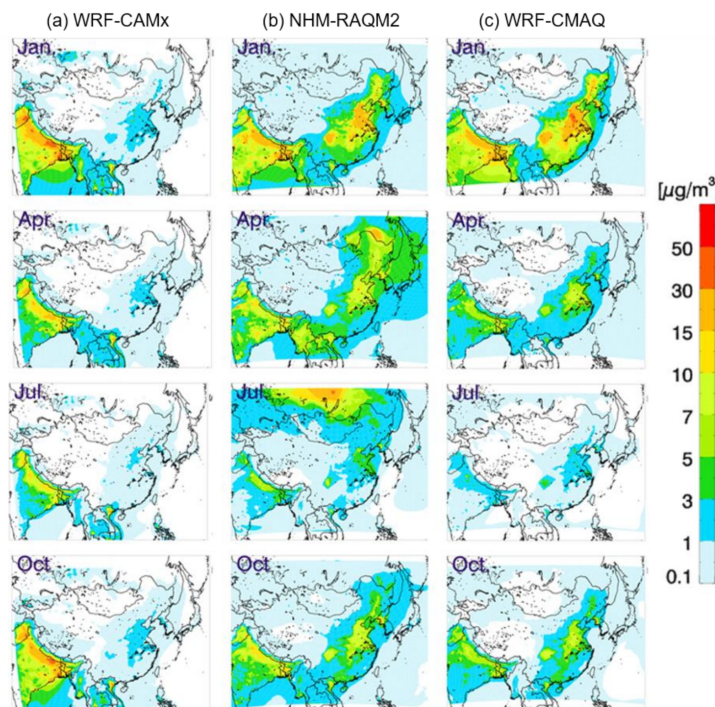


**Figure 5.** As in Figure 2, but for organic carbon (OC) concentrations ( $\mu\text{g}/\text{m}^3$ ).

The greatest difference occurs over southern Russia in July in the NHM-RAQM2 model, as indicated in Figure 5. As described above, this discrepancy is due to biomass burning emissions, which are considered only in NHM-RAQM2, leading to the most striking difference among the three models. Among the three models, WRF-CAMx predicted considerably lower OC concentrations with no particular monthly variation. Under the big seasonality, the highest concentration of OC simulated in winter over both central and northern China in this study is of interest, as OC levels in some areas exceeded  $40 \mu\text{g}/\text{m}^3$ . WRF-CMAQ simulated a maximum concentration of  $43.2 \mu\text{g}/\text{m}^3$  in January over an area near northern Shanghai in China; meanwhile, the maxima predicted with NHM-RAQM2 and WRF-CAMx were  $31.3$  and  $20.9 \mu\text{g}/\text{m}^3$ , respectively (Figure 5).

Generally, SOA model predictions have been underestimates in numerous previous studies [28–32]. This underestimation occurs due to uncertainty in estimating VOC volatility, which is related to the complex SOA generation mechanisms used for SOA simulation. Hence, the results of secondary OC formation simulations differ greatly according to the treatment of VOC volatility [31,33]. The underlying drivers of inter-model biases thus originate from the complexity of the SOA formation process, and the use of three different SOA formation modules in our study, as indicated in Table 1, might have directly caused the inter-model variability in OC distribution simulations (Figure 5).

**Elemental Carbon (EC) component:** The simulated EC distribution patterns (Figure 6) appear similar to those of OC, except that monthly average levels were generally lower than  $7 \mu\text{g}/\text{m}^3$  over the entire Northeast Asia domain. EC originates mainly from incomplete combustion in Asia [34], including combustion of both fossil fuels and biofuels. Our simulations of EC concentrations were higher (but less than 1) in winter ( $0.83 (\pm 0.67)\sim 3.33 (\pm 2.28 \mu\text{g}/\text{m}^3$ , respectively) and much lower in summer ( $0.34 (\pm 0.18)\sim 2.30 (\pm 1.15) \mu\text{g}/\text{m}^3$ , respectively), as illustrated in Figure 6. Inter-model bias remains apparent, related to complicated uncertainties; nevertheless, we believe that our EC results are worthwhile as a reference for estimating the monthly mean levels and spatial patterns over Northeast Asia, as no observational EC distributions are available that cover this domain at the regional or sub-regional scale.

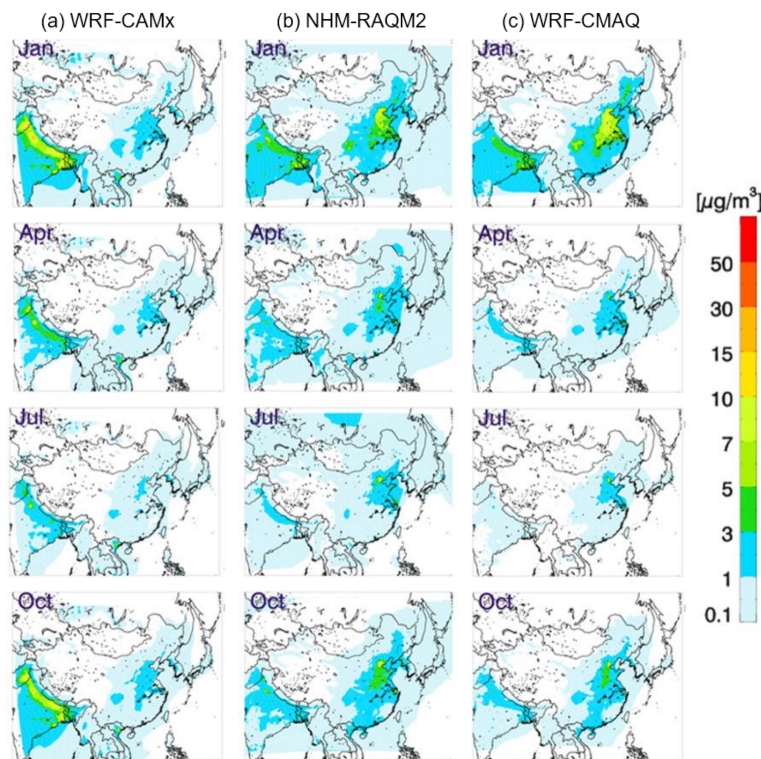


**Figure 6.** As in Figure 2, but for elemental carbon (EC) concentrations ( $\mu\text{g}/\text{m}^3$ ).

### 3.3. Model Validation against Observations over Exit-and-Entrance Areas

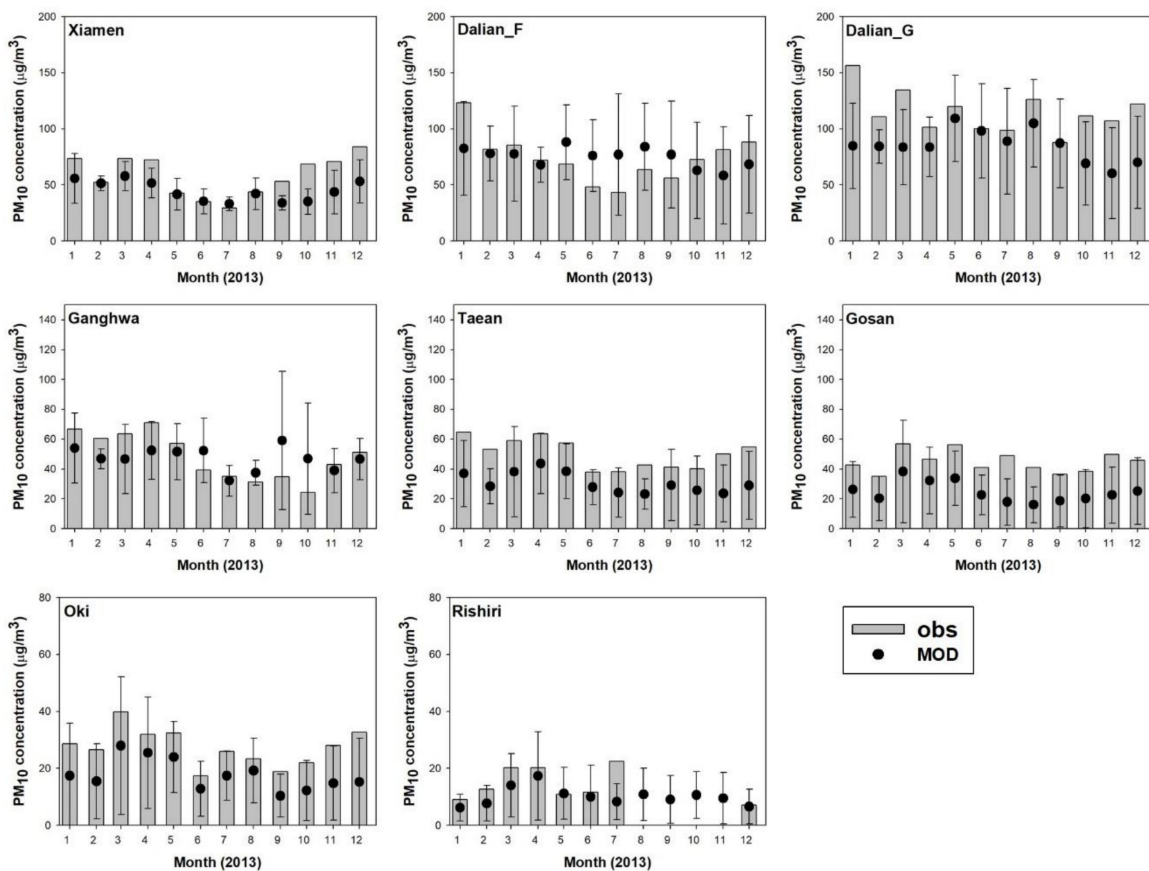
Supplementary Tables S3 and S4 summarize the statistical accuracy scores of simulated SO<sub>2</sub> and NO<sub>2</sub> concentrations relative to measurements taken at seven remote exit-and-entrance sites (Figure 1). The statistical parameters employed here are root mean square error (RMSE), normalized mean bias (NMB), normalized mean error (NME), fractional bias (FB), and fractional error (FE). In Supplementary Tables S3 and S4, similar NMB in both SO<sub>2</sub> and NO<sub>2</sub> were found at seven sites with the SO<sub>2</sub> NMB of  $0.9 \pm 0.6$  and NO<sub>2</sub> NMB of  $0.7 \pm 0.4$ . This finding indicates that potential uncertainties in secondary ammonium sulfate and nitrate formation both remain unexplored, affecting predictions of the inorganic aerosol conversion process over Northeast Asia.

Table 2 summarizes the statistical accuracy scores of simulated PM<sub>10</sub> concentrations over the exit-and-entrance sites. Note that, due to the lack of site-specific PM<sub>2.5</sub> observations for 2013 in the current study, PM<sub>10</sub> observations were used instead. At all sites, the three simulations produced differing ranges with a variety of similarities and differences. The statistical parameters of the simulated PM<sub>10</sub> levels were NME of  $0.44 \pm 0.20$ , RMSE of  $21.5 \pm 12.7 \text{ } \mu\text{g/m}^3$ , and FE of  $0.02 \pm 0.01$  respectively, at seven remote exit-and-entrance sites. However, with few exceptions of NHM-RAQM2, the simulations exhibited consistent tendencies toward underestimation at all exit-and-entrance sites with the negative NMB and FB values, demonstrating that simulation accuracy could be improved. In Japan, both FB and FE estimates indicated higher levels of error than in the other two countries, and both modeled and observed values were extremely low.

**Table 2.** Statistical summary of simulated and observed PM<sub>10</sub> levels over six exit-and-entrance sites related to transboundary transport over China, Japan, and Korea. Here, RMSE, NMB, NME, FB, and FE denote root mean square error, normalized mean bias, normalized mean error, fractional bias, and fractional error, respectively.

Sites	Model	RMSE	NMB	NME	FB	FE
Dalian (Fujiazhuang)	CAMx	41.43	-0.35	0.42	-0.02	0.03
	RAQM2	50.78	0.67	0.69	0.01	0.02
	CMAQ	16.17	-0.13	0.16	-0.01	0.01
Xiamen (Hongwen)	CAMx	27.39	-0.24	0.42	-0.01	0.02
	RAQM2	9.39	-0.02	0.16	-0.00	0.01
	CMAQ	24.07	-0.32	0.33	-0.01	0.01
Oki	CAMx	21.57	-0.65	0.66	-0.04	0.04
	RAQM2	7.54	0.20	0.22	0.01	0.01
	CMAQ	20.34	-0.71	0.72	-0.03	0.03
Rishiri	CAMx	10.67	-0.59	0.64	-0.06	0.07
	RAQM2	9.05	0.58	0.58	0.02	0.02
	CMAQ	4.71	-0.31	0.32	-0.01	0.02
Ganghwa	CAMx	19.82	-0.25	0.31	-0.01	0.02
	RAQM2	32.73	0.64	0.68	0.01	0.02
	CMAQ	14.22	-0.18	0.26	-0.07	0.01
Gosan	CAMx	36.05	-0.69	0.69	-0.04	0.04
	RAQM2	8.05	0.05	0.19	0.00	0.01
	CMAQ	26.79	-0.56	0.57	-0.02	0.02
Taean	CAMx	33.98	-0.54	0.55	-0.03	0.03
	RAQM2	7.92	0.11	0.22	0.00	0.01
	CMAQ	28.16	-0.53	0.53	-0.02	0.03

Figure 7 shows simulated and observed monthly variations in PM<sub>10</sub> concentrations at the seven exit-and-entrance sites. All three models underestimated PM<sub>10</sub> at most of the seven sites. The largest discrepancies were found in May–September at Dalian, where the model grid was located close to a large urban area. Ganghwa in September–October was associated with the second largest discrepancy in this study (Figure 7). The overall discrepancies between the simulations and measurements were estimated as being approximately 2.5 or less.



**Figure 7.** Observed and simulated monthly average PM<sub>10</sub> concentrations at exit-and-entrance sites in China, Japan, and Korea. The site locations and characteristics are indicated in Figure 1 and Supplementary Table S1.

The time series of the simulated and observed PM<sub>10</sub> at the seven sites are shown in Supplementary Figure S8. The time series from the three models exhibited strong seasonal variations, and were reasonably comparable with observations at Dalian, Xiamen, and Ganghwā; however, at most sites, the modeled values were considerably lower than the observed values. Supplementary Figure S9 shows scatter plot comparisons with measurements from all three models. The results indicate a linear relationship with slope of 0.3–1.0 and R<sup>2</sup> of 0.26–0.50, and simulations for each of the seven sites tended to be underestimates relative to observations, possibly due to missing source errors associated with natural sources. During the LTP meeting, it was noted that the largest missing source was expected to be soil dust, which was not considered in the current LTP study.

#### 4. Discussion on PM<sub>2.5</sub> Characteristics over Exit-and-Entrance Areas

Figure 8 shows the NO<sub>3</sub><sup>−</sup>/SO<sub>4</sub><sup>2−</sup> and OC/EC ratios for the four months over the model domain. In Figure 8a–d, significantly strong monthly variations in NO<sub>3</sub><sup>−</sup>/SO<sub>4</sub><sup>2−</sup> ratios of up to ~4.5 were simulated over most areas of Northeast Asia, including northern and southern China, and Seoul in Korea, but not Japan. The NO<sub>3</sub><sup>−</sup>/SO<sub>4</sub><sup>2−</sup> ratios are expected to have increased in China since 2013 due to significant SO<sub>2</sub> emission reduction strategies implemented in China starting in 2013 [35]; therefore, knowledge of recent changes in Chinese primary emissions is a prerequisite to further assessing possible air pollution control strategies in the region.

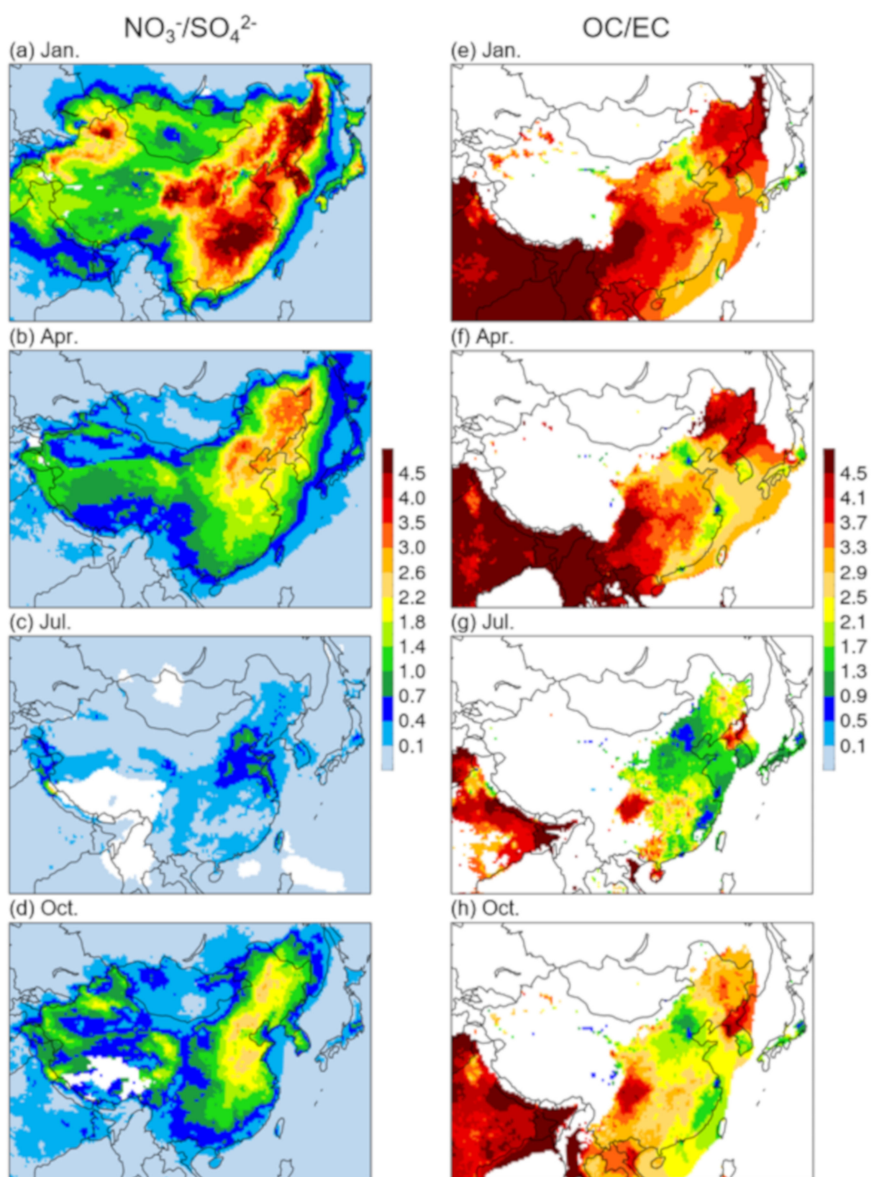


**Figure 8.** Spatial distributions of simulated monthly mean  $\text{NO}_3^-/\text{SO}_4^{2-}$  and OC/EC ratios for January (a,e), April (b,f), July (c,g), and October (d,h) in 2013.

The spatial distributions of the OC/EC ratios are shown in Figure 8e–h. Generally, OC and EC exhibit large and unique spatial and temporal variations (e.g., Figures 5 and 6). By contrast, consistent patterns in the OC/EC ratio are more easily found, partly because the ratio of these two chemicals tends to be less sensitive to atmospheric processes than their individual levels [36,37]. OC/EC ratios are generally lower in winter and higher in spring and summer. Monitoring studies have shown that the highest summer peak of ~10 occurs over the Northern Plains of China [38,39], relative to the mid- and north-eastern regions of China, whereas the lowest seasonal variation in the OC/EC ratio is found in the mid-western region.

Our simulations of OC/EC revealed opposite seasonal variations, with high values in winter and low in summer, due to the OC simulations shown in Figure 5. Domain-averaged OC/EC ratios over China–Korea–Japan were higher in winter ( $4.34 \pm 0.12$ ) and much lower in summer ( $0.74 \pm 0.18$ ), with a maximum of 4.6 in January (Figure 8e). In addition, a strong correlation between OC and  $\text{O}_3$  has been reported [40] and the temperature and solar radiation during summer are expected to increase SOA fractions to at least  $59\% \pm 11\%$  of total carbon aerosols in some places [41]. However, our study showed that there

was a weak correlation between EC and OC in summer over the three countries in the LTP domain ( $R^2 = 0.31$ , averaged from the three models in the current study), suggesting additional sources in our model domain combined with transport during other seasons. This weak association is also linked to uncertainties in organic simulations, including both primary and secondary aerosol formation processes. Nevertheless, over the entire year-long period, distinctively higher OC/EC ratios were found over northern provinces characterized by agriculture, as well as the entire North Korean territory.

In early 2013, emission mitigation actions were implemented by the Chinese government to fight air pollution over the major cities of China. In the following years, China achieved dramatic improvements in air quality, especially over high-emission areas [42–46]. Accordingly, numerous air quality monitoring reports have been released in the following years. Satellite observations, such as Ozone Monitoring Instrument NO<sub>2</sub> and SO<sub>2</sub> values, revealed marked decreases in signals, especially over the Central and East China regions, and AERONET aerosol optical depth (AOD) data revealed a trend of decreasing particulate air pollutant levels over Beijing [47,48]. Emission estimation studies have approximated the SO<sub>2</sub> and NO<sub>x</sub> emission decreases to be 10–14% per year in China, and a clear decrease in AOD can be observed over downwind regions.

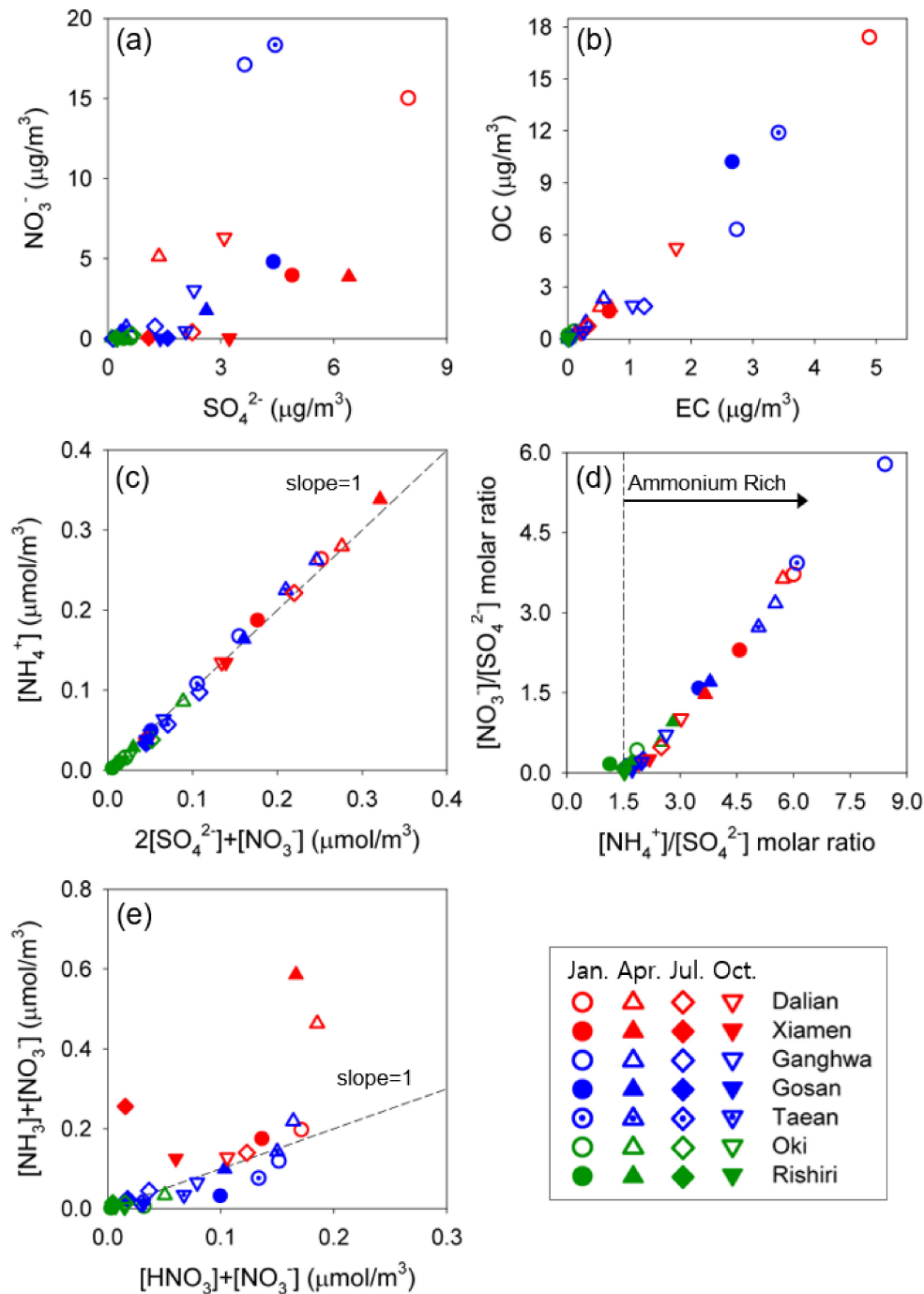
Based on recent in-situ PM<sub>2.5</sub> measurements, a notable pattern of decreasing SO<sub>4</sub><sup>2−</sup> and increasing NO<sub>3</sub><sup>−</sup> is present in China, especially during severe haze episodes [49–52], whereas extremely high NO<sub>3</sub><sup>−</sup> contributions have been frequently observed in source regions and downwind areas [49,53,54]. We aimed to explore the characteristics of PM<sub>2.5</sub> over exit-and-entrance areas. As no compound-specific observations were available for PM<sub>2.5</sub> in 2013, we only employed WRF-CMAQ simulations.

Figure 9a shows the simulated NO<sub>3</sub><sup>−</sup> and SO<sub>4</sub><sup>2−</sup> levels and their ratios over the seven remote sites. Dalian, an exit area in northern China, exhibited higher values (e.g., SO<sub>4</sub><sup>2−</sup> = 7.8 µg/m<sup>3</sup> in January), with a NO<sub>3</sub><sup>−</sup>/SO<sub>4</sub><sup>2−</sup> ratio of 1.8, indicating that NO<sub>3</sub><sup>−</sup> was higher than SO<sub>4</sub><sup>2−</sup> in 2013. However, over the Korean entrance sites (e.g., Ganghwa and Taean), tendencies of increasing NO<sub>3</sub><sup>−</sup> and decreasing SO<sub>4</sub><sup>2−</sup> were observed with relatively high NO<sub>3</sub><sup>−</sup>/SO<sub>4</sub><sup>2−</sup> ratios of 5.5–6.0 in January. This pattern of higher NO<sub>3</sub><sup>−</sup> over entrance areas indicates that air pollutants from the exit area in northern China are affected by atmospheric NH<sub>3</sub> during or after the LRT process, and that the re-establishment of gas-aerosol partitioning with semi-volatile species of ammonium nitrate can occur prior to the arrival of particulate ammonium nitrate over Korean entrance areas. On the other hand, Xiamen, an exit area in southern China, had approximately two-fold higher levels of SO<sub>4</sub><sup>2−</sup> than for NO<sub>3</sub><sup>−</sup> (e.g., in April) (Figure 9a). Over Japan, on the other hand, NO<sub>3</sub><sup>−</sup> and SO<sub>4</sub><sup>2−</sup> concentrations were extremely low, with values of less than 1 µg/m<sup>3</sup>.

OC and EC generally exhibited a consistent pattern, with OC/EC ratios of approximately 3:1 at most remote sites (Figure 9b). This OC/EC ratio, with a mean slope of more than 3, was higher than those reported in previous studies (e.g., OC/EC = 4–5 in Reference [39]), due to the fact that the underestimation of OC was less pronounced than that of EC.

We also attempted to interpret the combined effect of the percentages of SO<sub>4</sub><sup>2−</sup> and NO<sub>3</sub><sup>−</sup> associated with SIA formation over exit-and-entrance areas. Figure 9c shows the neutralization parameter,  $f_N$  ( $= [\text{NH}_4^+]/(2[\text{SO}_4^{2-}] + [\text{NO}_3^-])$ ), employed here for convenience [32,35,55]. Here,  $f_N = 1$  indicates an (NH<sub>4</sub>)<sub>2</sub>SO<sub>4</sub> sulfate aerosol (solid or aqueous), whereas  $f_N = 0.5$  indicates a bulk NH<sub>4</sub>HSO<sub>4</sub> sulfate aerosol [32,55]. Observations with  $f_N > 0.9$  indicate that SO<sub>4</sub><sup>2−</sup> was neutralized, whereas values of  $f_N > 1$  (excess aerosol NH<sub>4</sub><sup>+</sup>) cannot be reconciled based on SO<sub>4</sub><sup>2−</sup>–NO<sub>3</sub><sup>−</sup>–NH<sub>4</sub><sup>+</sup> aerosol thermodynamics, except for the neutralization of organic acids with NH<sub>3</sub> [56,57]. Our results showed that, whereas lower slopes of  $f_N$  were simulated over Rishiri and Oki, the slopes of  $f_N$  over the Chinese and Korean exit-and-entrance areas were generally  $\geq 1$ . This result indicates that the environment is favorable for SIA formation under NH<sub>3</sub>-sufficient conditions. This finding is also apparent in Figure 9d, where the ratios of  $([\text{NO}_3^-]/[\text{SO}_4^{2-}])/([\text{NH}_4^+]/[\text{SO}_4^{2-}])$  over most exit-and-entrance sites are  $> 10$ , indicating an “NH<sub>3</sub>-rich” regime, as described by

Pathak et al. [58]. This finding suggests that over remote areas, especially between China and Korea, the chemical conditions are favorable for SIA formation throughout Northeast Asia, with the exclusions of Rishiri and Oki in some months.



**Figure 9.** Simulated monthly mean (a)  $\text{NO}_3^- / \text{SO}_4^{2-}$  ratios, (b) OC/EC ratios, (c)  $[\text{NH}_4^+] / (2[\text{SO}_4^{2-}] + [\text{NO}_3^-])$ , (d)  $\text{NO}_3^-$ -to- $\text{SO}_4^{2-}$  molar ratios vs.  $\text{NH}_4^+$ -to- $\text{SO}_4^{2-}$  molar ratios, (e) adjusted gas ratios defined as  $([\text{NH}_4^+] + [\text{NO}_3^-]) / ([\text{HNO}_3] + [\text{NO}_3^-])$  at seven remote sites in China, Japan, and Korea.

Finally, Figure 9e shows the relationship  $([\text{NH}_3] + [\text{NO}_3^-])$  vs.  $([\text{HNO}_3] + [\text{NO}_3^-])$ , which indicates the “adjusted” gas ratio (AGR) of free  $\text{NH}_3$  to total  $\text{NO}_3^-$  [54]. This measure is another indicator of the sensitivity of the  $\text{NO}_3^-$  aerosol to changes in three types of emissions:  $\text{NH}_3$ ,  $\text{SO}_2$ , and  $\text{NO}_x$  [59–61]. Here,  $\text{AGR} < 1$  indicates an “ $\text{NH}_3$ -poor” regime, in which  $\text{NO}_3^-$  can be increased by replacing the decreased  $\text{SO}_4^{2-}$ , and  $\text{AGR} > 1$  (“ $\text{NH}_3$ -rich”

regime) indicates that  $\text{NO}_3^-$  is sensitive to changes in total  $\text{NO}_3^-$  ( $= [\text{HNO}_3] + [\text{NO}_3^-]$ ). In our study, as shown in Figure 9e, the exit areas of eastern China, such as Xiamen and Dalian, had high AGR values of 1 or more (especially in April), confirming the “ $\text{NH}_3$ -rich” condition of these areas. However, over the entrance area in Japan, the AGR indicates  $\text{NH}_4^+$ -poor conditions that make it impossible to establish a SIA-formation environment. This result suggests that gas-aerosol partitioning is likely to be established over Chinese exit areas affected by the observed levels of atmospheric  $\text{NH}_3$ . According to the results at the entrance area, the re-establishment of gas-aerosol partitioning is also likely to occur during the LRT process in the marine atmosphere between the exit and entrance areas. This partitioning can occur because the geographical locations of the Korean entrance areas are more than 500 km away from the Chinese exit areas, providing plentiful transit time to support the re-establishment of gas-aerosol partitioning.

Our findings in this study were inferred solely from modeling studies. Thus, our interpretation was affected by considerable uncertainties. In addition, further modeling sensitivity studies (with constraints on the thermodynamic modeling of aerosol composition) on the extent to which secondary aerosol formation is sensitive to  $\text{NH}_3$  and  $\text{HNO}_3$  levels are needed to help establish  $\text{PM}_{2.5}$  reduction strategies for the inflow and outflow regions of LRT pathways over China, Japan, and Korea.

## 5. Summary and Conclusions

The transboundary transport of PM in Northeast Asia has become a serious concern in recent years. Air pollutants emitted from upstream source areas can travel long distances to downstream regions, and therefore, the monitoring and characterization of such transboundary transport in exit-and-entrance areas over China, Japan, and Korea are of great importance. For this purpose, a cooperative project, namely the LTP project, has been conducted over a long time period by the governments of China, Korea, and Japan.

In this paper, we reported the results of long-term  $\text{PM}_{2.5}$  simulations covering an entire year, 2013, as agreed upon for the LTP project. Modeling groups from China, Japan, and Korea each employed their own modeling systems with conventional modeling options for the simulation of  $\text{PM}_{2.5}$  and associated species over the exit-and-entrance areas for LRT in Northeast Asia. The models employed by three countries are WRF-CAMx (by China), NHM-RAQM2 (by Japan), and WRF-CMAQ (by Korea), and their uncertainties in  $\text{PM}_{2.5}$  characterization were explored through comparison with surface measurements taken in 2013.

The results showed that some biases remain unexplored with the NME of  $0.44 \pm 0.20$  due to potential uncertainties in anthropogenic emission strengths and inherent model limitations. The general trends relative to observations over remote exit-and-entrance areas were the underestimation of  $\text{PM}_{10}$  monthly levels by a factor of 1.5–2.1. Among all tested models,  $\text{PM}_{2.5}$  concentrations exhibited similar seasonality, and the main difference was found in OC component among four chemical components of  $\text{PM}_{2.5}$ , especially in winter, and the second biggest discrepancy was in  $\text{NO}_3^-$  component for all of the three models.

Our analysis of several characteristics suggested a favorable environment for secondary inorganic  $\text{NO}_3^-$  formation over exit-and-entrance areas between China and Korea, with high  $\text{NH}_3$  gas concentrations. For the Japanese entrance areas, we were unable to fully explore the SIA characteristics due to the significantly low simulation values.

The characteristics of  $\text{PM}_{2.5}$  in 2013 analyzed in the current study are also expected to be important reference  $\text{PM}_{2.5}$  concentrations for further determining the impacts of Chinese emission mitigation policies on the improvement of air quality throughout Northeast Asia. The continuation of measurements of  $\text{PM}_{2.5}$  to quantitatively identify the influences of changes in emissions is expected, and the present study may provide foundational information on the characteristics of long-term  $\text{PM}_{2.5}$  modeling over Northeast Asia and the variability among model results.

In a future study, we plan to conduct further sensitivity analysis of  $\text{NH}_3$  or  $\text{HNO}_3$  reductions (achieved through  $\text{NO}_x$  control) to provide direction for efficient emission re-

duction strategies in Northeast Asia. The improvement of models for the robust estimation of SRRs will continue in the LTP modeling and monitoring research groups.

**Supplementary Materials:** The following are available online at <https://www.mdpi.com/article/10.3390/atmos12040469/s1>, Table S1: Characteristics of seven monitoring sites located in China, Japan, and Korea, Table S2: Total anthropogenic emissions (Tg/yr) from CREATE-2013 for China, Japan, and Korea over the model domain, Table S3: Statistical summary for SO<sub>2</sub> at seven monitoring sites in three countries, Table S4: Statistical summary for NO<sub>2</sub> at seven monitoring sites in three countries, Figure S1: Spatial distributions of CREATE-2013 emissions of selected species in the base year of 2013 (ton/yr/grid), Figure S2: Spatial distributions of monthly average temperature (°C) for January, April, July, and October 2013. The three air quality models are WRF-CAMx, NHM-RAQM2, and WRF-CMAQ, employed by China, Japan, and Korea, respectively, Figure S3: As in Figure S2, but for wind field (m/s), Figure S4: Scatter diagrams of modeled and observed temperatures at 2 m and wind speed at 10 m for the base year of 2013, Figure S5: Spatial distributions of monthly average SO<sub>2</sub> concentration (ppb) in January, April, July, and October 2013. Three air quality models?WRF-CAMx, NHM-RAQM2, and WRF-CMAQ, were employed by China, Japan, and Korea, respectively, Figure S6: As in Figure S5, but for NO<sub>2</sub> concentration (ppb), Figure S7: As in Figure S5, but for NH<sub>4</sub><sup>+</sup> concentration (μg/m<sup>3</sup>), Figure S8: Time series of simulated (red lines) and observed (black dots) daily mean PM<sub>10</sub> concentrations at seven monitoring sites. Three air quality models?WRF-CAMx, NHM-RAQM2, and WRF-CMAQ, were employed by China, Japan, and Korea, respectively, Figure S9: Scatter plots of daily mean modeled versus observed PM<sub>10</sub> in exit-and-entrance areas associated with transboundary transport over China, Japan, and Korea.

**Author Contributions:** Conceptualization, C.-H.K., F.M., and J.L.; Methodology, M.K., W.T., J.-J.L., and Y.K.; Data curation, J.-H.W., K.S., T.K., and H.M.; Formal analysis, J.K., K.-B.L., S.R., H.-Y.J., and Y.-J.J.; Investigation, C.-H.K., and J.L.; Visualization, J.-J.L., H.-Y.J., and Y.-J.J.; Writing—Original draft, C.-H.K.; Writing—Review and editing, F.M., and J.L. All authors have read and agreed to the published version of the manuscript.

**Funding:** This work was supported by a grant from the National Institute of Environment Research (NIER), funded by the Ministry of Environment (MOE) of the Republic of Korea (Grant No. NIER-2018-01-02-037), and also by the Research Foundation of Korea (NRF) of the Ministry of Education of the Republic of Korea (Grant No. 2020R1A6A1A03044834).

**Institutional Review Board Statement:** Not applicable.

**Informed Consent Statement:** Not applicable.

**Data Availability Statement:** Data are available upon request.

**Acknowledgments:** The authors acknowledge all of modeling sub-working group members not listed as co-authors in this paper but who participated in the 21st LTP expert meeting in 2018 organized by Korea, China, and Japan for LTP discussions. Also, the authors thank the researchers from NIER (National Institute of Environmental Research, South Korea), CRAES (Chinese Research Academy of Environmental Sciences, China), and ACAP (Asia Center for Air Pollution Research, Japan) for both carrying out the models and providing the measurement for model verification. Special thanks are given to anonymous reviewers for their helpful comments.

**Conflicts of Interest:** The authors declare no conflict of interest.

## References

- Chiashi, A.; Lee, S.; Pollitt, H.; Chewpreecha, U.; Vercoulen, P.; He, Y.; Xu, B. Transboundary PM Air Pollution and Its Impact on Health in East Asia. In *Energy, Environmental and Economic Sustainability in East Asia: Policies and Institutional Reforms*; Lee, S., Pollitt, H., Fujikawa, K., Eds.; Routledge: London, UK, 2019.
- Kim, C.-H.; Park, S.-Y.; Kim, Y.-J.; Chang, L.-S.; Song, S.-K.; Moon, Y.-S.; Song, C.-K. A Numerical Study on Indicators of Long-range Transport Potential for Anthropogenic Particle Matter over Northeast Asia. *Atmos. Environ.* **2012**, *58*, 35–44. [[CrossRef](#)]
- Latza, U.; Gerdes, S.; Baur, X. Effects of Nitrogen Dioxide on Human Health: Systematic Review of Experimental and Epidemiological Studies Conducted between 2002 and 2006. *Int. J. Hyg Environ. Health* **2009**, *212*, 271–287. [[CrossRef](#)] [[PubMed](#)]
- Sunyer, J.; Basagana, X.; Belmonte, J.; Anto, J.M. Effect of Nitrogen Dioxide and Ozone on the Risk of Dying in Patients with Severe Asthma. *Thorax Int. J. Respir. Med.* **2002**, *57*, 687–693. [[CrossRef](#)] [[PubMed](#)]

5. Vedal, S.; Brauer, M.; White, R.; Petkau, J. Air Pollution and Daily Mortality in a City with Low Levels of Pollution. *Environ. Health Perspect.* **2003**, *111*, 45–52. [[CrossRef](#)]
6. Li, Z.; Chen, H.; Cribb, M.; Dickerson, R.; Holben, B.; Li, C.; Lu, D.; Luo, Y.; Maring, H.; Shi, G.; et al. Preface to Special Section on East Asian Studies of Tropospheric Aerosols: An International Regional Experiment (EASTAIRE). *J. Geophys. Res. Atmos.* **2007**, *112*, D22S00. [[CrossRef](#)]
7. Lee, H.-J.; Jo, H.-Y.; Park, S.-Y.; Jo, Y.-J.; Jeon, W.; Ahn, J.-Y.; Kim, C.-H. A Case Study of the Transport/Transformation of Air Pollutants over the Yellow Sea during the MAPS 2015 Campaign. *J. Geophys. Res. Atmos.* **2019**, *124*, 6532–6553. [[CrossRef](#)]
8. Choi, K.-C.; Lee, J.-J.; Bae, C.-H.; Kim, C.-H.; Chang, L.-S.; Ban, S.-J.; Lee, S.-J.; Kim, J.; Woo, J.-H. Assessment of Transboundary Ozone Contribution toward South Korea Using Multiple Source-receptor Modeling Technique. *Atmos. Environ.* **2014**, *92*, 118–129. [[CrossRef](#)]
9. Kim, C.-H.; Chang, L.-S.; Kim, J.-S.; Meng, F.; Kajino, M.; Ueda, H.; Zhang, Y.; Son, H.-Y.; He, Y.; Xu, J.; et al. Long-term Simulations of the Sulfur Concentrations over the China, Japan and Korea: A Model Comparison Study. *Asia Pac. J. Atmos. Sci.* **2011**, *47*, 399–411. [[CrossRef](#)]
10. Kim, C.-H.; Chang, L.-S.; Meng, F.; Kajino, M.; Ueda, H.; Zhang, Y.; Son, H.-Y.; Lee, J.-J.; He, Y.; Xu, J.; et al. Sulfur Deposition Simulations over China, Japan and Korea: A Model Intercomparison Study for Abating Sulfur Emission. *Environ. Sci. Pollut. Res.* **2012**, *19*, 4073–4089. [[CrossRef](#)]
11. Park, I.-S.; Choi, W.-J.; Lee, T.-Y.; Lee, S.-J.; Han, J.-S.; Kim, C.-H. Simulation of long-range transport of air pollutants over Northeast Asia using a comprehensive acid deposition model. *Atmos. Environ.* **2005**, *39*, 4075–4085. [[CrossRef](#)]
12. Jin, Y.; Andersson, H.; Zhang, S. Air Pollution Control Policies in China: A Retrospective and Prospects. *Int. J. Environ. Res. Public Health* **2016**, *13*, 1219. [[CrossRef](#)]
13. Zhang, L.; Brook, J.R.; Vet, R. A revised parameterization for gaseous dry deposition in air-quality models. *Atmos. Chem. Phys.* **2003**, *3*, 2067–2082. [[CrossRef](#)]
14. An, J.; Ueda, H.; Wang, Z.; Matsuda, K.; Kajino, M.; Cheng, X. Simulations of Monthly Mean Nitrate Concentrations in Precipitation over East Asia. *Atmos. Environ.* **2002**, *36*, 4159–4171. [[CrossRef](#)]
15. Byun, D.W.; Ching, J.K.S. *Science Algorithms of the EPA Models-3 Community Multiscale Air Quality (CMAQ) Modeling System*; EPA Report; EPA/600/R-99/030; EPA: Washington, DC, USA, 1999.
16. ENVIRON. *CAMx User's Guide Version 6.2*; Environ International Corporation: Novato, CA, USA, 2015.
17. Han, Z.; Ueda, H.; Sakurai, T. Model Study on Acidifying Wet Deposition in East Asia during Wintertime. *Atmos. Environ.* **2006**, *40*, 2360–2373. [[CrossRef](#)]
18. Kajino, M.; Inomata, Y.; Sato, K.; Ueda, H.; Han, Z.; An, J.; Katata, G.; Deushi, M.; Maki, T.; Oshima, N.; et al. Development of the RAQM2 Aerosol Chemical Transport Model and Predictions of the Northeast Asian Aerosol Mass, Size, Chemistry, and Mixing Type. *Atmos. Chem. Phys.* **2012**, *12*, 11833–11856. [[CrossRef](#)]
19. Wei Wang, C.B.; Duda, M.; Dudhia, J.; Gill, D.; Kavalich, M.; Keene, K.; Chen, M.; Lin, H.; Michalakes, J.; Rizvi, S.; et al. *ARW Version 3 Modeling System User's Guide*; NCAR: Boulder, CO, USA, 2016.
20. Saito, K.; Ishida, J.; Aranami, K.; Hara, T.; Segawa, T.; Narita, M.; Honda, Y. Nonhydrostatic Atmospheric Models and Operational Development at JMA. *J. Meteorol. Soc. Jpn.* **2007**, *85B*, 271–304. [[CrossRef](#)]
21. Kim, C.-H.; Lee, H.-J.; Kang, J.-E.; Jo, H.-Y.; Park, S.-Y.; Jo, Y.-J.; Lee, J.-J.; Yang, G.-H.; Park, T.; Lee, T. Meteorological Overview and Signatures of Long-range Transport Processes during the MAPS-Seoul 2015 Campaign. *Aerosol Air Qual. Res.* **2018**, *18*, 2173–2184. [[CrossRef](#)]
22. Kurokawa, J.; Ohara, T.; Morikawa, T.; Hanayama, S.; Janssens Maenhout, G.; Fukui, T.; Kawashima, K.; Akimoto, H. Emissions of Air Pollutants and Greenhouse Gases over Asian Regions during 2000–2008: Regional Emission Inventory in Asia (REAS) Version 2. *Atmos. Chem. Phys.* **2013**, *13*, 11019–11058. [[CrossRef](#)]
23. Giglio, L.; Randerson, J.T.; van der Werf, G.R.; Kasibhatla, P.S.; Collatz, G.J.; Morton, D.C.; DeFries, R.S. Assessing Variability and Long-term Trends in Burned Area by Merging Multiple Satellite Fire Products. *Biogeosciences* **2010**, *7*, 1171–1186. [[CrossRef](#)]
24. Volkamer, R.; Jimenez, J.L.; Martini, F.S.; Dzepina, K.; Zhang, Q.; Salcedo, D.; Molina, L.T.; Worsnop, D.R.; Molina, M.J. Secondary Organic Aerosol Formation from Anthropogenic Air Pollution: Rapid and Higher Than Expected. *Geophys. Res. Lett.* **2006**, *33*, L17811. [[CrossRef](#)]
25. Yang, G.-H.; Jo, Y.-J.; Lee, H.-J.; Song, C.-K.; Kim, C.-H. Numerical Sensitivity Tests of Volatile Organic Compounds Emission to PM<sub>2.5</sub> Formation during Heat Wave Period in 2018 in Two Southeast Korean Cities. *Atmosphere* **2020**, *11*, 331. [[CrossRef](#)]
26. Li, B.; Zhang, J.; Zhao, Y.; Yuan, S.; Zhao, Q.; Shen, G.; Wu, H. Seasonal Variation of Urban Carbonaceous Aerosols in a Typical City Nanjing in Yangtze River Delta, China. *Atmos. Environ.* **2015**, *106*, 223–231. [[CrossRef](#)]
27. Zhou, J.; Xiong, Y.; Xing, Z.; Deng, J.; Du, K. Characterizing and Sourcing Ambient PM<sub>2.5</sub> over Key Emission Regions in China II: Organic Molecular Markers and CMB Modeling. *Atmos. Environ.* **2017**, *163*, 57–64. [[CrossRef](#)]
28. Bhave, P.V.; Pouliot, G.A.; Zheng, M. Diagnostic Model Evaluation for Carbonaceous PM<sub>2.5</sub> Using Organic Markers Measured in the Southeastern U.S. *Environ. Sci. Technol.* **2007**, *41*, 1577–1583. [[CrossRef](#)]
29. Carlton, A.G.; Bhave, P.V.; Napelenok, S.L.; Edney, E.O.; Sarwar, G.; Pinder, R.W.; Houyoux, M. Model Representation of Secondary Organic Aerosol in CMAQv4.7. *Environ. Sci. Technol.* **2010**, *44*, 8553–8560. [[CrossRef](#)]
30. Henze, D.K.; Seinfeld, J.H. Global Secondary Organic Aerosol from Isoprene Oxidation. *Geophys. Res. Lett.* **2006**, *33*, L09812. [[CrossRef](#)]

31. Yu, S.; Bhate, P.V.; Dennis, R.L.; Mathur, R. Seasonal and Regional Variations of Primary and Secondary Organic Aerosols over the Continental United States: Semi-empirical Estimates and Model Evaluation. *Environ. Sci. Technol.* **2007**, *41*, 4690–4697. [[CrossRef](#)]
32. Zhang, Q.; Jimenez, J.L.; Worsnop, D.R.; Canagaratna, M. A Case Study of Urban Particle Acidity and Its Influence on Secondary Organic Aerosol. *Environ. Sci. Technol.* **2007**, *41*, 3213–3219. [[CrossRef](#)]
33. Lee, H.-J.; Jo, H.-Y.; Song, C.-H.; Jo, Y.-J.; Park, S.-Y.; Kim, C.-H. Sensitivity of Simulated PM<sub>2.5</sub> Concentrations over Northeast Asia to Different Secondary Organic Aerosol Modules during the KORUS-AQ Campaign. *Atmosphere* **2020**, *11*, 1004. [[CrossRef](#)]
34. Bond, T.C.; Doherty, S.J.; Fahey, D.W.; Forster, P.M.; Berntsen, T.; DeAngelo, B.J.; Flanner, M.G.; Ghan, S.; Karcher, B.; Koch, D.; et al. Bounding the Role of Black Carbon in the Climate System: A Scientific Assessment. *J. Geophys. Res.* **2013**, *118*, 5380–5552. [[CrossRef](#)]
35. Jo, Y.-J.; Lee, H.-J.; Jo, H.-Y.; Woo, J.-H.; Kim, Y.; Lee, T.; Heo, G.; Park, S.-M.; Jung, D.; Park, J.; et al. Changes in Inorganic Aerosol Compositions over the Yellow Sea Area from Impact of Chinese Emissions Mitigation. *Atmos. Res.* **2020**, *240*, 104948. [[CrossRef](#)]
36. McKeen, S.A.; Liu, S.C. Hydrocarbon Ratios and Photochemical History of Air Masses. *Geophys. Res. Lett.* **1993**, *20*, 2363–2366. [[CrossRef](#)]
37. Wang, Y.; Zeng, T. On Tracer Correlations in the Troposphere: The Case of Ethane and Propane. *J. Geophys. Res.* **2004**, *109*, D24306. [[CrossRef](#)]
38. Liu, Z.R.; Gao, W.K.; Yu, Y.C.; Hu, B.; Xin, J.Y.; Sun, Y.; Wang, L.L.; Wang, G.H.; Bi, X.H.; Zhang, G.H.; et al. Characteristics of PM<sub>2.5</sub> Mass Concentrations and Chemical Species in Urban and Background Areas of China: Emerging Results from the CARE-China Network. *Atmos. Chem. Phys.* **2018**, *18*, 8849–8871. [[CrossRef](#)]
39. Ji, D.; Gao, M.; Maenhaut, W.; He, J.; Wu, C.; Cheng, L.; Gao, W.; Sun, Y.; Sun, J.; Xin, J.; et al. The Carbonaceous Aerosol Levels Still Remain a Challenge in the Beijing-Tianjin-Hebei Region of China: Insights from Continuous High Temporal Resolution Measurements in Multiple Cities. *Environ. Int.* **2019**, *126*, 171–183. [[CrossRef](#)] [[PubMed](#)]
40. Ye, Z.; Li, Q.; Ma, S.; Zhou, Q.; Gu, Y.; Su, Y.; Chen, Y.; Chen, H.; Wang, J.; Ge, X. Summertime Day-night Differences of PM<sub>2.5</sub> Components (Inorganic Ions, OC, EC, WSOC, WSON, HULIS, and PAHs) in Changzhou, China. *Atmosphere* **2017**, *8*, 189. [[CrossRef](#)]
41. Zhao, B.; Wang, S.; Donahue, N.M.; Jathar, S.H.; Huang, X.; Wu, W.; Hao, J.; Robinson, A.L. Quantifying the Effect of Organic Aerosol Aging and Intermediate-volatility Emissions on Regional-scale Aerosol Pollution in China. *Sci. Rep.* **2016**, *6*, 28815. [[CrossRef](#)] [[PubMed](#)]
42. Krotkov, N.A.; McLinden, C.A.; Li, C.; Lamsal, L.N.; Celarier, E.A.; Marchenko, S.V.; Swartz, W.H.; Bucsela, E.J.; Joiner, J.; Duncan, B.N.; et al. Aura OMI Observations of Regional SO<sub>2</sub> and NO<sub>2</sub> Pollution Changes from 2005 to 2015. *Atmos. Chem. Phys.* **2016**, *16*, 4605–4629. [[CrossRef](#)]
43. Liu, F.; Zhang, Q.; van der Ronald, J.; Zheng, B.; Tong, D.; Yan, L.; Zheng, Y.; He, K. Recent Reduction in NO<sub>x</sub> Emissions over China: Synthesis of Satellite Observations and Emission Inventories. *Environ. Res. Lett.* **2016**, *11*, 114002. [[CrossRef](#)]
44. Zhang, J.; Reid, J.S.; Alfaro-Contreras, R.; Xian, P. Has China Been Exporting Less Particulate Air Pollution over the Past Decade? *Geophys. Res. Lett.* **2017**, *44*, 2941–2948. [[CrossRef](#)]
45. Zhao, B.; Jiang, J.H.; Gu, Y.; Diner, D.; Worden, J.; Liou, K.N.; Su, H.; Xing, J.; Garay, M.; Huang, L. Decadal-scale Trends in Regional Aerosol Particle Properties and Their Linkage to Emission Changes. *Environ. Res. Lett.* **2017**, *12*, 054021. [[CrossRef](#)]
46. Zheng, B.; Tong, D.; Li, M.; Liu, F.; Hong, C.; Geng, G.; Li, H.; Li, X.; Peng, L.; Qi, J.; et al. Trends in China’s Anthropogenic Emissions since 2010 as the Consequence of Clean Air Actions. *Atmos. Chem. Phys.* **2018**, *18*, 14095–14111. [[CrossRef](#)]
47. Gu, X.; Bao, F.; Cheng, T.; Chen, H.; Wang, Y.; Guo, H. The Impacts of Regional Transport and Meteorological Factors on Aerosol Optical Depth over Beijing, 1980–2014. *Sci. Rep.* **2018**, *8*, 5113. [[CrossRef](#)]
48. Li, J. Pollution Trends in China from 2000 to 2017: A Multi-sensor View from Space. *Remote Sens.* **2020**, *12*, 208. [[CrossRef](#)]
49. Tian, M.; Wang, H.B.; Chen, Y.; Zhang, L.M.; Shi, G.M.; Liu, Y.; Yu, J.Y.; Zhai, C.Z.; Wang, J.; Yang, F.M. Highly Time-resolved Characterization of Water-soluble Inorganic Ions in PM<sub>2.5</sub> in a Humid and Acidic Mega City in Sichuan Basin, China. *Sci. Total Environ.* **2017**, *580*, 224–234. [[CrossRef](#)]
50. Tian, M.; Liu, Y.; Yang, F.; Zhang, L.; Peng, C.; Chen, Y.; Shi, G.; Wang, H.; Luo, B.; Jiang, C.; et al. Increasing Importance of Nitrate Formation for Heavy Aerosol Pollution in Two Megacities in Sichuan Basin, Southwest China. *Environ. Pollut.* **2019**, *250*, 898–905. [[CrossRef](#)]
51. Wang, J.; Zhao, B.; Wang, S.; Yang, F.; Xing, J.; Morawska, L.; Ding, A.; Kulmala, M.; Kerminen, V.-M.; Kujansuu, J.; et al. Particulate Matter Pollution over China and the Effects of Control Policies. *Sci. Total Environ.* **2017**, *584*, 426–447. [[CrossRef](#)]
52. Yang, F.; Tan, J.; Zhao, Q.; Du, Z.; He, K.; Ma, Y.; Duan, F.; Chen, G.; Zhao, Q. Characteristics of PM<sub>2.5</sub> Speciation in Representative Megacities and Across China. *Atmos. Chem. Phys.* **2011**, *11*, 5207–5219. [[CrossRef](#)]
53. Li, H.; Zhang, Q.; Zheng, B.; Chen, C.; Wu, N.; Guo, H.; Zhang, Y.; Zheng, Y.; Li, X.; He, K. Nitrate-driven Urban Haze Pollution during Summertime over the North China Plain. *Atmos. Chem. Phys.* **2018**, *18*, 5293–5306. [[CrossRef](#)]
54. Yang, T.; Sun, Y.; Zhang, W.; Wang, Z.; Liu, X.; Fu, P.; Wang, X. Evolutionary Processes and Sources of High-nitrate Haze Episodes over Beijing, Spring. *J. Environ. Sci.* **2017**, *54*, 142–151. [[CrossRef](#)]
55. Fisher, J.A.; Jacob, D.J.; Wang, Q.; Bahreini, R.; Carouge, C.C.; Cubison, M.J.; Dibb, J.E.; Diehl, T.; Jimenez, J.L.; Leibensperger, E.M.; et al. Sources, Distribution, and Acidity of Sulfate-ammonium Aerosol in the Arctic in Winter-spring. *Atmos. Environ.* **2011**, *45*, 7301–7318. [[CrossRef](#)]

56. Dinar, E.; Anttila, T.; Rudich, Y. CCN Activity and Hygroscopic Growth of Organic Aerosols Following Reactive Uptake of Ammonia. *Environ. Sci. Technol.* **2008**, *42*, 793–799. [[CrossRef](#)] [[PubMed](#)]
57. Mensah, A.A.; Buchholz, A.; Mentel, T.F.; Tillmann, R.; Kiendler-Scharr, A. Aerosol Mass Spectrometric Measurements of Stable Crystal Hydrates of Oxalates and Inferred Relative Ionization Efficiency of Water. *J. Aerosol Sci.* **2011**, *42*, 11–19. [[CrossRef](#)]
58. Pathak, R.K.; Wu, W.S.; Wang, T. Summertime PM<sub>2.5</sub> Ionic Species in Four Major Cities of China: Nitrate Formation in an Ammonia-deficient Atmosphere. *Atmos. Chem. Phys.* **2009**, *9*, 1711–1722. [[CrossRef](#)]
59. Pinder, R.W.; Dennis, R.L.; Bhave, P.V. Observable Indicators of the Sensitivity of PM<sub>2.5</sub> Nitrate to Emission Reductions—part I: Derivation of the Adjusted Gas Ratio and Applicability at Regulatory-relevant Time Scales. *Atmos. Environ.* **2008**, *42*, 1275–1286. [[CrossRef](#)]
60. Dennis, R.L.; Bhave, P.V.; Pinder, R.W. Observable Indicators of the Sensitivity of PM<sub>2.5</sub> Nitrate to Emission Reductions—Part II: Sensitivity to Errors in Total Ammonia and Total Nitrate of the CMAQ-predicted Non-linear Effect of SO<sub>2</sub> Emission Reductions. *Atmos. Environ.* **2008**, *42*, 1287–1300. [[CrossRef](#)]
61. Wang, J.; Xu, J.; He, Y.; Chen, Y.; Meng, F. Long Range Transport of Nitrate in the Low Atmosphere over Northeast Asia. *Atmos. Environ.* **2016**, *144*, 315–324. [[CrossRef](#)]